RSC Advances

REVIEW

View Article Online
View Journal | View Issue

Cite this: *RSC Adv.*, 2023, **13**, 18070

Surface modified nanoparticles and their applications for enantioselective detection, analysis, and separation of various chiral compounds

Susanti, [a] Asep Riswoko, *[a] Joddy Arya Laksmono, [a] Galuh Widiyarti [b] and Dadan Hermawan [c]

Received 11th April 2023
Accepted 30th May 2023

DOI: 10.1039/d3ra02399k

rsc.li/rsc-advances

The development of efficient enantioselective detection, analysis, and separation relies significantly on molecular interaction. In the scale of molecular interaction, nanomaterials have a significant influence on the performance of enantioselective recognitions. The use of nanomaterials for enantioselective recognition involved synthesizing new materials and immobilization techniques to produce various surface-modified nanoparticles that are either encapsulated or attached to surfaces, as well as layers and coatings. The combination of surface-modified nanomaterials and chiral selectors can improve enantioselective recognition. This review aims to offer engagement insights into the production and application of surface-modified nanomaterials to achieve sensitive and selective detection, better chiral analysis, and separation of numerous chiral compounds.

1 Introduction

Enantioselective detection, analysis, and separation are important because of the different activities of each enantiomer. For example, in the pharmaceutical fields, enantiomers of chiral drug compounds have different pharmacodynamic, pharmacokinetic, and toxicological properties.[1–4] Identifying the enantiomer of a chiral compound is essential when assessing the quality of food, *i.e.*, the existence of (D)-amino acid in natural substances may suggest an indication that bacterial contamination has occurred.[5] Besides, it is crucial for other

[a]*Research Center for Polymer Technology – National Research and Innovation Agency (BRIN), KST BJ. Habibie, Kawasan Puspiptek Building 460, Tangerang Selatan, 15314, Indonesia. E-mail: asep022@brin.go.id*

[b]*Research Center for Pharmaceutical Ingredients and Traditional Medicine – National Research and Innovation Agency (BRIN), KST BJ Habibie, Kawasan Puspiptek Building 452, Tangerang Selatan, 15314, Indonesia*

[c]*Department of Chemistry, Faculty of Mathematics and Natural Science, Jenderal Soedirman University (UNSOED), Indonesia*

Susanti received her PhD from the University of Groningen in 2018. Her thesis title is Enantioselective liquid–liquid extraction in microreactors. She is working as a postdoctoral research fellow at The National Research and Innovation Agency (BRIN) in Indonesia. Her interest in chirality issues was initiated when she took a research program for her master's degree at the University of Technology Malaysia. Her research focuses now on chiral separation, especially by leveraging recent advances in nanoscience and nanotechnology.

Asep Riswoko is a senior researcher at National Research and Innovation Agency, Indonesia with thirty years of experience in downstreaming research results to the public. He received his PhD from Saitama University, Japan in 2001. Specializing in molecular design and synthesis to produce optically active compound needed for pharmaceutical industry and agriculture.

fields like agrochemicals, flavor, fragrance, *etc.* Many chemical pesticides exist as racemates (enantiomers mixtures of a chiral compound), which poses a potential risk to aquatic life and humans because it might be only one of two enantiomers that has an active site in pest control.[6,7] In flavor, (*R*)-asparagine provides a sweet flavor, whereas (*S*)-asparagine gives a bitter taste to humans.[8] Another instance in fragrance is the enantiomeric pair of carvone, where (*R*)-carvone has a mint odor, and (*S*)-carvone has a caraway smell.[9]

Enantiomerically pure compounds can be obtained through asymmetric synthesis, racemic mixture separation, or natural sources (chiral pool).[10,11] The synthesis of single enantiomers through asymmetric synthesis is a well-established technique. Nonetheless, it is not ideal for large-scale production and is limited to specific enantioselective reactions.[12,13] Synthesizing chiral compounds in their racemic form is relatively simple than synthesizing pure enantiomers directly, so effective enantiomeric separation (enantioseparation) is required.[13–15]

Numerous methods have been reported for enantioseparation, including laboratory methods like chromatography and capillary electrophoresis.[14,16–18] Although needing significant capital investments for scale-up,[10,19] the enantioseparation of small amounts of racemates is required in the initial development stages. Examples of preparative chiral separation methods are centrifugal partition chromatography,[20] simulated moving bed chromatography,[21–23] crystallization,[24–26] membrane-based approaches,[27–29] and liquid–liquid extraction (LLE).[30–33] Each methods possesses distinctive capability in enantioseparation. Crystallization is a commonly used method to obtain enantiopure compounds, but it is limited for the case of conglomerate systems and requires significant handling of solid materials.[25]

The development of enantioseparation through available methods is being explored to get a good enantioseparation of chiral compounds. Typically, a good enantioseparation is marked by the high selectivity, sensitivity, stability, and efficiency of enantioselective separation itself. The enantioseparation performance is often presented in terms resolution (Rs), selectivity factor (α) and or enantiomeric excess (ee). The ee can be calculated following the equation below:

$$\text{Enantiomeric excess (ee)} = \frac{|[\text{R}] - [\text{S}]|}{[\text{R}] + [\text{S}]} \times 100\%$$

where [R] and [S] are the concentrations of the (*R*)- and (*S*)-enantiomer in the solution.

Achieving efficient separation of enantiomers remains challenging due to the inherent obstacles associated with these techniques. This difficulty primarily arises because enantiomer pairs possess nearly identical physiochemical properties.[12,34] Moreover, most of the available methods necessitate using costly chiral selector and or chiral column.[35] Therefore, every method of development usually involves either developing the new chiral selector and or modifying of an available chiral selector.

Enantioseparation occurs due to differences in complexation between enantiomers and a chiral selector. According to the principle of enantiomeric recognition, also known as the three-point rule, a minimum of three intermolecular interactions among enantiomers and a chiral selector are required for the

Joddy Arya Laksmono is a senior researcher at Research Center for polymer technology – National Research and Innovation Agency. He received his PhD from the Doctoral study in chemical Engineering Department, Faculty of Engineering – Universitas Indonesia in 2019. Since his master's degree, he has an interest and focuses in the development of nanomaterials and their modifications via chemical coordinations route, and then prepares the materials to become composites for certain functions, especially for separation and purification processes.

Galuh Widiyarti is a senior researcher at Research Center for Pharmaceutical Ingredients and Traditional Medicine BRIN. She graduated from the doctoral study of the chemistry department of Universitas Indonesia in 2017. Her research topic being worked is the separation of active compounds from natural products for anti-oxidant, anti-diabetic, anti-inflammatory and anti-cancer pharmaceutical ingredients. Currently, the focus of her research is the synthesis and modification of nanoparticle materials for the chiral compounds separation as an anti-inflammatory drug.

Dadan Hermawan is a lecturer and researcher at Jenderal Soedirman University (UNSOED), Indonesia. He earned his PhD from the University of Technology Malaysia (UTM) in 2009. After completing his PhD, he conducted postdoctoral research on the chiral separation of various compounds using capillary electrophoresis (CE) at UTM. His research focuses on separation, sensing biomolecules, and nanomaterials. He has a specific interest in chiral analysis using CE and chromatographic methods.

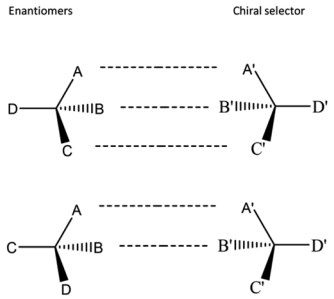

Fig. 1 Schematic illustration of the three-point rule.[36]

proper configuration of the complex.[35–37] One of these interactions, relying on the stereochemical aspects, impacts the different interactions for both enantiomers with a chiral selector.[37] Intermolecular interactions include hydrogen bonding, dipole–dipole interactions, π–π interactions, ion pairs interactions, hydrophobic interactions, as well as host-guest inclusion interactions. The three-point rule is schematically shown in Fig. 1.

Enhancing the selectivity, sensitivity, and stability of molecular interaction between enantiomers and a chiral selector will result in high efficiency of enantioselective separation. Rather than using a bulk compound of chiral selector and enantiomer, attaching each of them to the surface of a nanoparticle could enhance the selectivity, stability, and efficiency of enantioselective recognition, including enantioselective detection, analysis, and separation, which are reported in many publications.[5,12,34,35,38]

The use of nanomaterials such as nanoparticles and nanotubes offer a new approach to enantioselective recognition. The combinations of nanomaterials and a chiral selector can be adjusted to enhance their ability to detect and distinguish between enantiomers, which makes them highly suitable for enantiomeric recognition and separation.[12,35] This paper covers a brief description of nanomaterials in general resumes the benefits and remaining challenges of using nanoparticles through surface modification in enantioselective detection, analysis, and separation.

2 Nanomaterials

According to The International Organization for Standardization (ISO), "nanomaterial" is defined as a "material with any external dimension in the nanoscale or having an internal structure or surface structure in the nanoscale" (ISO, 2010), where nanoscale is the size range from approximately 1–100 nm (ISO, 2008).[39] Based on the ISO definition, Krug and Wick[40] described and classified nanomaterials as depicted in Fig. 2. Fig. 2 shows that nanomaterials can be nanoobjects or nanostructured materials. Nanoobjects are discrete pieces of material with one or more outer dimensions in the nanoscale. In comparison, nanostructured materials have their internal or surface structure in the nanoscale dimension.

Based on dimensionality, there are three classes of nanoobjects, *i.e.*, nanoparticles, nanofibers, and nanoplates. Nanoparticles are substances with a size that measures in the nanoscale in all three dimensions. Moreover, nanofibers and nanoplates are materials with two and one dimensions in the nanoscale, respectively. In addition, nanofibers include different types, such as hollow nanofibers called nanotubes, rigid nanofibers known as nanorods, and electrically conductive nanofibers known as nanowires.

Nanomaterials classifications were also reported based on their source, consecutive or composition materials, potential toxicity, and other parameters.[34,41] The detailed nanomaterials classifications have been covered by Saleh *et al.*[41] and Vassal *et al.*[42] In recent years, the classifications of nanomaterials have mostly been reported based on their applications.

The distinctive characteristics of nanomaterials, such as their diverse sizes, shapes, functionalities, customizable surfaces, and biocompatibility, make them highly versatile and applicable in various fields.[12,34,35] Nanotechnology can utilize this at small scales to create the desired properties. For example, they are making a material lighter, more durable,

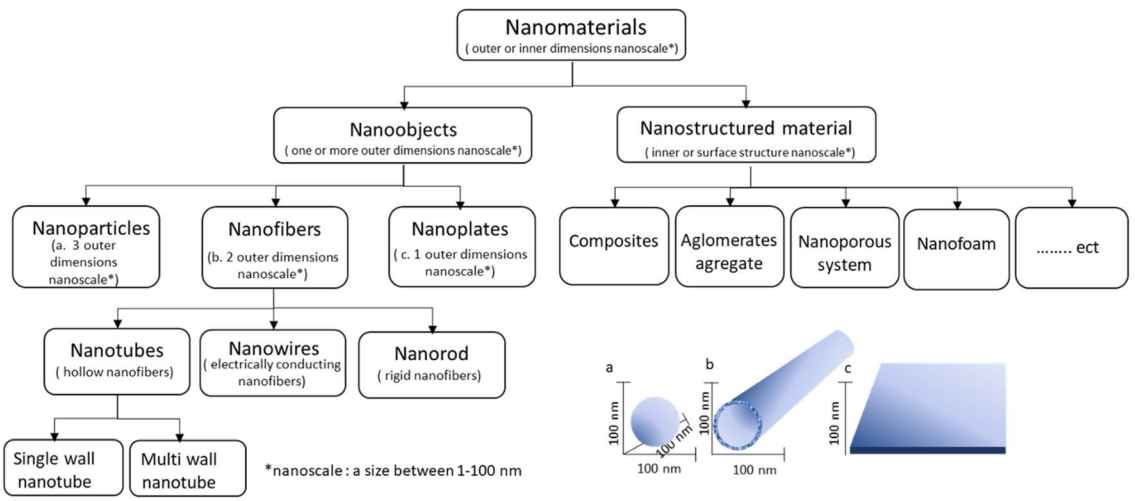

Fig. 2 Nanomaterials based on ISO definition. Adapted from ref. 40. (© 2011 Wiley-VCH Verlag GmbH & Co. KGaA, Weinheim).

more reactive, *etc.* Several fields have utilized the advantages of the nanomaterials, such as in various branches of science, biomedicine, cancer diagnosis, the food industry, and others.[34,43–45]

Besides these advantages of nanomaterials for many applications in modern technology, there are limitations to the use of nanomaterials in terms of its hinder solubility, poor dispersion in an aqueous system, low bonding availability, and so on, if the nanomaterial is not treated before using.[46] For this reason, nanomaterial properties should be tuned as desired *via* appropriate functionalization or surface modification. Through this process, in the past few decades, nanomaterials have been actively used in enantioselective recognition and enantioselective separation.[34,45]

3 The utilization of nanomaterials in enantioselective recognition

Enantioselective recognition is of utmost importance process because of its significant role in numerous applications, such as chiral sensors, chiral analysis, enantioseparation, and other related fields.[47] Various surface-modified nanomaterials, including nanoparticles, nanotubes, and nanoporous, in combination with a chiral selector, have improved enantioselective recognition in enantioselective detection, enantioselective analysis, and enantioseparation of different racemic.[5,12,34,35,38]

3.1 Metallic nanoparticles

Metallic nanoparticles, typically gold and silver-based nanoparticles, are primarily used in sensing or detection of a chiral compound through enantioselective colorimetry, enantioselective analysis by capillary electrophoresis (CE), or HPLC. A summary of the combination of either gold nanoparticles (AuNPs) or silver nanoparticles (AgNPs) with the chiral selector and their performance is provided in Table 1.

3.1.1 Gold-based nanomaterials. Many reasons for gold-based nanomaterials are used widely in enantioselective recognition, especially in detection and analysis. Gold-based nanomaterials have unique optical characteristics with various shapes and sizes, easy for surface modification, and have high biocompatibility.[48–50] Since their colorimetric assays are very sensitive, that is easier to detect color change. In addition, gold-based nanomaterials can be customized to the desired specifications by carefully controlling the morphological and reaction characteristics to the expected size and shape of gold nanoparticles (AuNPs) such as nanosphere, nanorod, nanocage, and nanoflower.[12,34]

The application of gold-based nanomaterials has been reported in several publications. The application for enantiomeric recognition, mostly AuNP modified with cysteine (Cys) and its variant as a chiral selector due to the sulfur group in cysteine being able to bind readily to the NP surface.[34] Cys-modified AuNPs were successfully achieved for enantiomeric recognition of several compounds such as propylene oxide,[51] naproxen,[52] 3,4-dihydroxyphenylalanine,[53] propranolol,[54] and tyrosine.[55]

AuNPs modified with either D- or L-Cys, following two different methods, *i.e.*, exposing the AuNPs to Cys 24 h after their synthesis and exposing the AuNPs to Cys during their synthesis.[51] Both methods give similar results. The performance of Cys-modified AuNPs has been probed using polarimetry. L-Cys-modified AuNPs preferred to adsorb the (*R*)-propylene oxide, whereas D-Cys-modified AuNPs adsorbed (*S*)-propylene oxide.[51] Cys-modified AuNPs selectively adhere to one enantiomer, which causes the other enantiomer to be more concentrated in the solution.

L-Cys-capped AuNPs have been investigated for colorimetric enantioselective detection of naproxen (NAP)[52] and D,L-3,4-dihydroxyphenylalanine (Dopa).[53] In the presence of (*R*)-NAP, the color of L-Cys-capped AuNPs changes from red to blue, whereas the presence of (*S*)-NAP does not affect their color (see Fig. 3).[52] The changing color was observed, *i.e.*, from red to blue, when the L-DOPA was present in the L-Cys-capped AuNPs solution, while the color remained the same with the presence of D-DOPA.[53] The aggregation or disaggregation of colloidal gold nanoparticles in solution caused the changes in the surface plasmon absorption band.[56] This can be conveniently utilized to convert the recognition of molecules at a molecular level into a measurable signal, *i.e.*, the color change.[56] The color change from red to blue is characteristic of using AuNPs for colorimetry, even in unmodified AgNPs.[57]

Furthermore, D- and L-cys-modified AuNPs have been used to measure the solutions containing (*R*,*S*)-propanolol (PLL).[54] The study employed tetrahexahedral of AuNPs (THH AuNPs). Using optical polarimetry was observed D- and L-cys-modified THH–AuNPs preferred to bind (*R*)- and (*S*)-PLL, respectively. The results show the equilibrium constant for adsorption of (*R*)-PLL to L-cys-modified THH–AuNPs is 2.2 times that of (*S*)-PLL.[54] Additionally, the binding of (*S*)-PLL to L-cys modified THH–AuNPs is 2.2 times that of (*R*)-PLL.[54]

The cysteine variant, *N*-acetyl-L-cysteine (NALC), was capped with AuNPs for L-tyr detection.[55] NALC–AuNPs were capable of visually enriching L-tyr. Meanwhile, L-tyr induced the aggregation of AuNPs and separated from the solution through centrifugation, thus leaving behind a clear liquid.[55] In a control experiment, *i.e.*, with the D-tyr addition, most of the gold nanoparticles remained in the solution even when centrifuged under identical conditions. It indicates NALC–AuNPs could selectively separate racemic tyr solution because D-tyr could not be extracted from the solution.[55]

For enantioselective separation, Liu *et al.*[58] reported the use of bovine serum albumin (BSA) modified AuNPs for enantioseparation of dansyl-norvaline. BSA was immobilized on gold nanoparticles capped silica (AuNPs@SiO_2) as a chiral stationary phase (CSP) on the HPLC column. The CSP successfully separated the racemic of Dansyl-norvaline with the best resolution (Rs) of 1.3 in only 5 cm of column length. Furthermore, Huang *et al.* demonstrated a quick preparative separation method for enantiomers of tryptophan, D,L-tryptophan, using AuNP modified with functional nucleic acids.[59] Sequentially, a portion of aptamer-functionalized AuNPs (apt-AuNPs) was added into

Table 1 Metallic-based nanoparticles in the identification and separation of enantiomers

Core/shell	Chiral selector	Chiral compound(s)	Separation/detection	Remarks	Ref.
AuNP	(D)- or (L)-cysteine (Cys)	Propylene oxide	Optical polarimetry	Av diameter AuNPs ~5 nm. (L)-cys- and (D)-cys-modified AuNPs preferred to adsorb the (*R*)- and (*S*)-propylene oxide, respectively	51
AuNPs	(L)-Cys	Naproxen (NAP) racemic	Colorimetry	The red color of (L)-cys capped Au NPs solution changes to blue in the existence of (*R*)-NAP. However, no color changes were observed in the existence of (*S*)-NAP	52
AuNP	(L)-Cys	(D,L)-3,4-Dihydroxy-phenylalanine (Dopa)	Colorimetry	(L)-Cys-modified AuNPs preferred to adsorb (L)-DOPA it can be observed by the change solution color from red to blue when the (L)-DOPA enantiomer present in the (L)-Cys-modified AUNPs solution, while the (D)-DOPA not affected the color change	53
AuNP	(D)- or (L)-cys	Propranolol (PLL)	Optical polarimetry	Shape rod-like with $D \sim 40$ nm and length 100 nm. The binding of (*S*)-PLL to the surfaces of (L)-cys/THH–Au NPs is 2.2 times that of (*R*)-PLL	54
AuNP	Chiral *N*-acetyl-(L)-cys	(D,L)-tyr	Colorimetry & TEM	Size ranges from 6-8 nm. Only L-tyr selectively induced aggregation of NALC–Au NPs	55
AuNP	—	(D,L)-Tryptophan (Trp)	Colorimetry	The presence of (D)-Trp shows a noticeable change in the color solution of AuNPs from red to blue, while the presence of (L)-Trp does not cause any color change. However, the AuNP probe can detect (D)-Trp in the range of 0.2–10 μM	57
AuNPs@SiO_2	BSA	Dansyl-norvaline	HPLC	The best Rs of 1.3 was obtained in a 5 cm column	58
AuNP	Nucleic acid aptamers	(D,L)-Trp	CE	Aptamer-functionalized AuNPs selectively adsorb (L)-Trp. Complete separation was obtained after five times of adding aptamer-functionalized AuNPs to the racemic solution	59
AuNPs	Streptomycin	Adrenaline, noradrenaline, and isoprenaline	CE	Rs up to 7.5 was obtained in 7 min	60
AuNPs	(D)-Penicillamine	Amlodipine (AML), tropicamide (TRO), and ofloxacin (OFL)	CE	Av size of synthesized particles was 3–5 nm. Rs AML increased from 0.92 to 1.97, Rs TRO improved from 0.66 to 1.17, and Rs OFL increased from 0.74 to 1.58	61
AuNPs	Thiolated β-CD	(D,L)-Valine (Val), leucine (Leu), glutamic acid (Glu), aspartic acid (Asp), chlorpheniramine, zopiclone and carvedilol	Pseudostationary phase-CEC	Av. diameter NPs was 9.5 ± 2.5 nm. Rs of 2.5, 2.7, 3.8, and 1.7 for (D,L)-Glu, (D,L)-Asp, (D,L)-Leu, and (D,L)-Val, respectively. While Rs of chlorpheniramine, zopiclone, and carvedilol, were 2.9, 4.7, and 2.0, respectively	62
AgNPs	Sulfonated β-CD	1-Phe-1-propanol, 1-Phe-2-propanol, and 2-phe-1-propanol	CE	Size AgNPs ~21 nm. In the presence of AgNPs, it was obtained Rs 2.18 (1-phe-1-propanol), 1.00 (1-phe-2-propanol), and 8.7 (2-phe-1-propanol)	64
AgNPs	Nucleotide uridine 50-triphosphate (UTP)	(D,L)-Cys	Colorimetry	It qualitatively indicated UTP-capped AgNPs selectively interacted with (D)-cys than (L)-cys	65
AgNPs	Citrate	(D,L)-Trp	Colorimetry	The solution color shifted from yellow to red when (D)-Trp was present, but there was no color change in the presence of (L)-Trp. From the measurements obtained, the ee range between 50–100% for (D)-Trp	123

Table 1 (*Contd.*)

Core/shell	Chiral selector	Chiral compound(s)	Separation/detection	Remarks	Ref.
AgNPs	Sulfonated-substituted zinc tetraphenylporphyrin (ZnTPPS) and L-Arg	(D,L)-Histidine	Colorimetry	The presence of (L)-Histidine causes a noticeable alteration in color, shifting from brown-yellow to red. The color of the solution does not appear to be affected by the presence of (D)-histidine	124
AgNPs	Chitosan	(D,L)-Trp	Colorimetry and scanometry	The average diameter size of chitosan-capped AgNPS is 15 ± 2 nm. CS-AgNPs yellowish solution changed to brown in the presence of (L)-Trp, whereas (D)-Trp did not cause a color change	63
AgNPs	β-CD	(D,L)-Phe, (D,L)-Trp, and (D,L)-Tyr	Colorimetry	β-CD-modified AgNPs were selectively adsorbed (D)-Phe, or (L)-Trp, and or (L)-tyr. β-CD-modified AgNPs solution color changed from yellow to red with their presence	125
AgNPs@SiO_2	Cellulose tris-(3,5-dimethylphenylcarbamate)	Fifteen racemates of chiral drugs	HPLC	Eight of fifteen studied analytes reached baseline separation (Rs > 1.5) at each optimum condition, *i.e.*, 2-phenyl-cyclohexanone, benzoin, praziquantel, (D,L)-benzylpenicillin, *trans*-stilbene oxide, cypermethrin, (*R*,*S*)-equol and ibuprofen	66

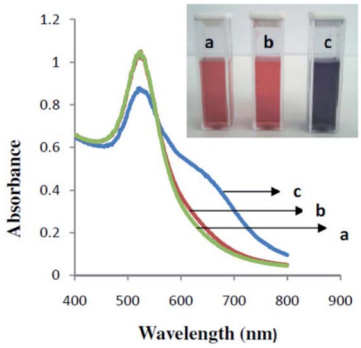

Fig. 3 UV-vis absorption spectra of (L)-cys-capped AuNPs (a) and (L)-cys-capped AuNPs in the existence of (*S*)-naproxen (b) and (*R*)-naproxen (c).[52] (© The Royal Society of Chemistry 2015).

(D,L)-Trp solution (0.5 mM). After five rounds of adding apt-AuNPs and centrifugation, (L)-Trp was entirely separated from the original mixture of (D,L)-Trp.

Several studies reported AuNPs usage for enantioseparation in capillary electrophoresis (CE) systems. AuNPs are favored to improve the enantioseparation performance in CE due to their distinctive chemical surface, which can produce a steady suspension in the electrolyte background. As a chiral selector, Streptomycin modified AuNPs (ST-AuNPs) was successfully used for enantioseparation of adrenergic compounds using CE.[60] Under ideal conditions, the separation achieved a baseline separation of the analytes in just seven minutes with Rs up to 7.5, indicating a highly effective separation.[60] Another study used D-penicillamine functionalized AuNPs (D-Pen-AuNPs) combined with hydroxypropyl-β-cyclodextrin (HP-β-CD) in the enantioseparation of amlodipine, tropicamide, and ofloxacin in CE system.[61] Compared to the use of bare HP-β-CD, the addition of D-Pen-AuNPs has improved the Rs. Rs of AML increased from 0.92 to 1.97, Rs TRO from 0.66 to 1.17, and Rs OFL from 0.74 to 1.58.[61] Fig. 4 schematically represents the recognition mechanism along the capillary channel. In this case, the presence of AuNPs caused better interaction between one of the enantiomers with the chiral selector. The results of their interactions increased the difference in their migrations in the electric field.

Yang *et al.*[62] used AuNPs for enantioseparations of various compounds in another mode of CE, *i.e.*, pseudo stationary phase-capillary electrochromatography (PSP-CEC), with thiolated-β-cyclodextrin as a chiral selector (CS). In the paper, it was nice to compare the use of CS with and without the presence of AuNPs. The separation resolutions (Rs) of studied analytes in the optimum concentration of thiolated-β-CD-modified AuNPs (0.30–0.53 mM in BGE) were 2.9 (chlorpheniramine), 4.7 (zopiclone), and 2.0 (carvedilol), while no separation by using the same amount of pure β-CD. Accordingly, the Rs improved with the presence of AuNPs. The Rs at the optimum concentration of thiolated-β-CD-modified AuNPs were comparable with the results using the optimum concentration of pure β-CD (15 mM).[62] Thus, the use of CS with the presence of AuNPs was much lower than without the presence of AuNPs.

The mentioned studies show that nanoparticles improved enantioselective analysis and enantioseparation even with

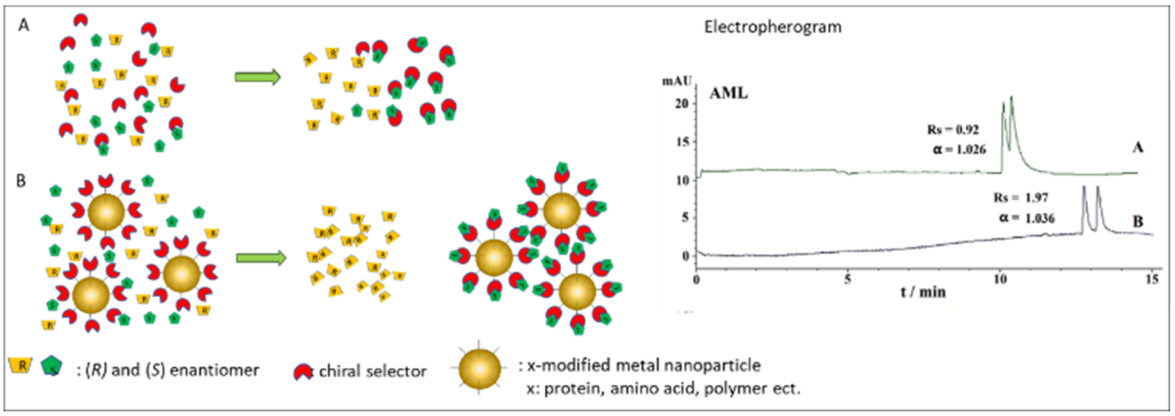

Fig. 4 Schematic illustration of recognition mechanism in CE system with and without the presence of metal nanoparticles. AML electropherogram was obtained with permission from ref. 61 (© 2020 WILEY-VCH Verlag GmbH & Co. KGaA, Weinheim).

reducing chiral selector concentration. The use of AuNPs improved colorimetric detection mainly due to their optical sensitivity. Accordingly, chiral recognition can be observed easily without specialized equipment. Furthermore, the enantioseparation is enhanced because chiral selector-modified nanoparticles present a large surface area, allowing better contact and interaction with the analytes.

3.1.2 Silver-based nanomaterials. The utilization of silver nanoparticles (AgNPs) for chiral identification and enantioseparation is not as much as AuNPs. AgNPs have exceptional photochemical and photophysical characteristics, and their ability to excite plasmons efficiently has led to their growing use as colorimetric sensors to identify chiral molecules.[63] However, functionalizing them caused chemical deterioration, resulting in lower stability of AgNPs than AuNPs.[34]

Several synthesis methods of Ag-NPs have been reported, including chemical, physical, photochemical, and biological procedures. However, considering factors such as the expenses, scalability, particle size, and size distribution, chemical methods offer a convenient approach for producing nanoparticles in solution.[41] The next paragraph resume some published study regarding the use of AgNPs for chiral identification and enantioseparation of a chiral compound.

Choi *et al.* in 2005 used AgNPs for enantioseparation of Arylalcohol compounds in the CE systems.[64] AgNPs were added to the background electrolyte consisting of a chiral selector, *i.e.*, sulfonated-β-CD. The presence of AgNPs improved the separation (Rs) of 1-phenyl-1-propanol, 1-phenyl-2-propanol, and 2-phenyl-1-propanol from 0.18 to 2.18, from 0.16 to 1.00, and from 0.17 to 8.7, respectively.[64]

AgNP in colorimetric discrimination of cysteine (Cys) enantiomers was reported by Zhang and co-workers.[65] The surface of AgNPs is modified with nucleotide uridine 50-triphosphate (UTP). A transparent 384-well microtiter plate was used for the investigation. UTP-modified AgNPs aliquot in supporting solutions and buffer were placed in the wells of the microtiter plate. The absorption reading was started immediately after the addition of the (L)-Cys or (D)-Cys to the corresponding wells.[65] Moreover, the enantioselective induction of AgNP aggregation is achieved through an enantiomer of Cys. The other enantiomer remains in excess in the solution, leading to enantioseparation and a quick colorimetric enantiodiscrimination of Cys without specialized instruments. Accordingly, the UTP-modified AgNPs prefer (D)-cys compared to (L)-Cys.[65]

Another study reported the use of AgNPs to modify the chiral stationary phase (CSP) for the enantioseparation of fifteen chiral drugs.[66] SiO_2@Ag particles were produced from functionalized porous silica core and AgNPs as the shell *via* the seed growth technique. The surfaces of SiO_2@Ag particles were modified with cellulose derivatives (as chiral selectors, CS) through the coating and intermolecular polycondensation to create CSPs.[66] The study compared the performance of CSPs prepared with and without AgNP modification. The use of SiO_2@Ag particles for separation resulted in increased interaction with the analytes and better enantioseparation.[66]

Likewise, using AuNPs, the use of AgNPs improved the selectivity in chiral discrimination and enantioseparation. In some cases, the presence of nanoparticles also improved the separation performance faster than the one without their presence. The main reason is due to the high surface area provided by the nanoparticles.

3.2 Metal oxide-based nanoparticles

Nanoparticles made of metal oxides, including magnetite (Fe_3O_4), titania (TiO_2), and zirconia (ZrO_2), are also beneficial for enantioseparation purposes.[35] The ease of handling and manipulation of metal oxide nanoparticles surface with a desired chiral selector become favorable for chiral discrimination and enantioseparation. Additionally, the use of magnetic nanoparticles offers other benefits, including high capacity for adsorption, rapid adsorption rate, minimal adsorbent quantity, quick equilibrium time to adsorb analytes, and easy collection of complexes from the solution.[12,34,35,38] Accordingly, compared with the conventional separation methods, employing magnetic nanoparticles enables the enantioseparation to become faster, easier, and cost-effective.[34]

Among metallic oxide-based materials, iron oxide magnetite (Fe_3O_4) is the most applied magnetics material in separation

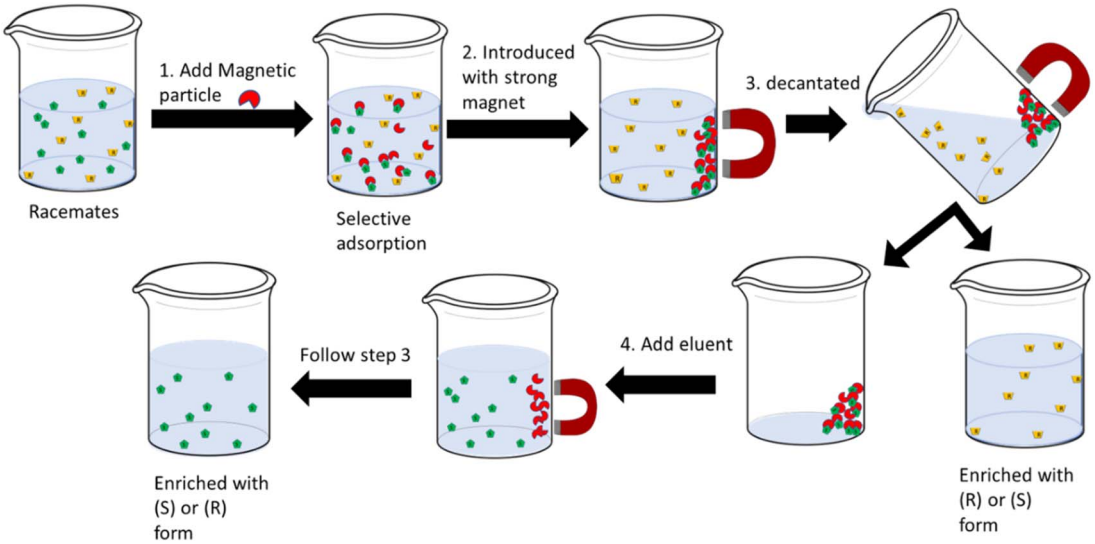

Fig. 5 The use of magnetic nanoparticles in solid phase extraction of racemate solution.

science, including enantioseparation. The reason for this is primarily because of their simple procedures of fabrication.[35,67] Their small size offers a vast surface area leading to high extraction capacity and relatively short extraction time.[45,67] The other important character is their superparamagnetic characteristics which makes them easy to be separated directly with the help of an external magnet, as illustrated in Fig. 5. Fig. 5 represents the use of magnetic particles in solid phase extraction of racemates solution.

The formation of agglomerates from magnetic nanoparticles (m-NPs) easily oxidizable in the air becomes a drawback of the use of m-NPs.[45] To prevent the formation of agglomerates and to improve the stability of m-NPs, one of the most prevalent tactics employed is to shield them with a coating, such as a core–shell configuration.[45] According to Deng and co-workers, the production process for m-NPs consisted of three distinct stages: creating a magnetic core, coating or protecting the core, and modifying the surface of the resulting core–shell structure (see Fig. 6).[35]

Several materials have been used for coating the magnetic core, including silica, alumina, carbon (including graphene and carbon nanotubes [CNTs]), zirconia, and polymers such as polystyrene, polydopamine, polynoerpineprine, *etc.* Silica is one of the most widely used for coatings or modifying m-NPs surface. The reasons are likely because of the low cost, chemical stability, mechanical and chemical robustness, thermal stability, and ease of surface modification.[45] When silica is applied as a coating to an m-NP, the abundance of silanol groups on its surface enables simple surface customization using other organic or inorganic functional groups or materials, including a chiral selector that is utilized for enantioseparation.[45]

The functionalization of mNPs depends on the analytes being separated. Several chiral selectors have been employed, including cyclodextrin,[68–75] polymers,[76–80] proteins,[81–85] amino acids,[86–88] and cellulose.[89–91] Cyclodextrin-functionalized mNPs are mostly used for the separation of amino acid enantiomers. All cited papers used β-CD and its derivatives, which may be caused by the inner cavity of β-CD providing the most compatible size for target amino acids compared to α-CD and γ-CD. Considering that the CD cavity possesses chirality, it is reasonable to anticipate the occurrence of enantioselectivity when chiral substrates form complexes within the cyclodextrin cavity.[36] Based on the theory of guest–host inclusion complex, the enantiomers (guests) that occupy the chiral cavity to the fullest extent demonstrate the highest level of chiral recognition by the host (chiral selector).[36] In addition, It is also possible to have combinations of binding forces and chiral cavities. Therefore, the use of CD derivatives is an option to provide better selectivity in separating enantiomers. Ghosh *et al.* succeeded in the use of magnetic nanoparticles (mNPs) for the separation of (D,L)-tryptophan enantiomers with obtained ee more than 90%. The mNPs were explored by functionalizing

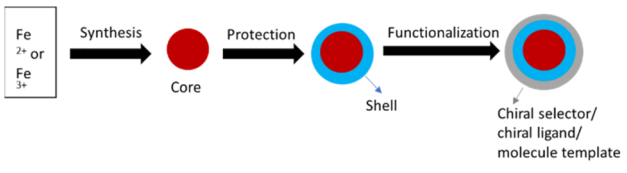

Fig. 6 Synthesis of magnetic-based nanomaterials adapted from ref. 35 (Copyright © Taylor & Francis Group, LL).

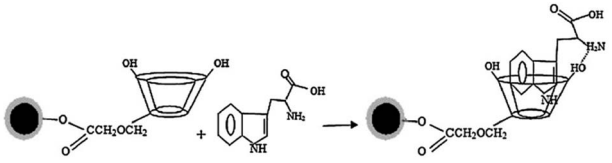

Fig. 7 Simplified schematic diagram showing adsorption mechanism of Trp onto Fe_3O_4/SiO_2/CMCD MNPs.[71] (© 2013 Elsevier B.V. All rights reserved).

Table 2 Metal oxide-based Nanoparticles in the identification and separation of enantiomers

Core/Shell	Chiral selector	Chiral compound(s)	Separation/detection	Remarks	Ref.
Fe_3O_4	β-CD	Alanine (Ala), Trp, tyr	Optical polarimetry	β-CD modified Fe_3O_4 nanoparticles mostly absorbed (L)-Trp more than (D)-Trp	68
Fe_3O_4/SiO_2	Carboxymethyl-β-CD (CM-β-CD)	Tryptophan (Trp), phenylalanine (Phe), tyrosine (Tyr)	UV-vis	Qualitatively the resolution predicts from the absorption capacity: (L)-Trp > (L)-Phe > (L)-tyr and (D)-Trp > (D)-Phe > (D)-tyr	69
GO/Fe_3O_4	β-CD	Trp	OT-CE	Av size about 8 nm. Trp enantiomers resolution was 1.65 and was achieved within 50 s	70
Fe_3O_4-PS	Helical substituted polyacetylene	1-Phenylethylamine	Optical rotation measurement	Adsorption of the (*R*)-form was much higher than the (*S*)-form of 1-phenylethylamine, *e.g.*, 24.60% at 12 h, compared to 1.76%	76
Fe_3O_4/SiO_2	CM-β-CD	Trp, Phe, Tyr	HPLC-UV	ee for separation (D,L)-Trp, (D,L)-Phe, and (D,L)-Tyr racemic were 94%, 73%, and 58%, respectively	71
Fe_3O_4/SiO_2	Amine functionalized derivatives β-CD (AmCD)	*N*-(3,5-Dinitrobenzoyl) phenlglycine, *N*-(1-phenylethyl) phthalamic acid	HPLC-UV	Am-CD-MNPs preferred to adsorb (*S*)-form enantiomer, *i.e.*, about 50% for (*S*)-phenylglycine and 30% for (*S*)-phthalamic acid, while the (*R*)-form was not carried	72
Fe_3O_4	BSA	Ibuprofen, ofloxacin	HPLC-UV	Av size ~13.3 nm. At single-stage operation, ee value of racemic ibuprofen and ofloxacin was 13% and 14%, respectively. The multistage process enhances the ee value up to 54% and 39%, respectively	81
GO/Fe_3O_4	BSA	Trp, threonine, propranolol	OT-CE	Rs of Trp, threonine, and propranolol were 1.22, 1.9, and 2.1, respectively	82
Fe_3O_4@Au	BSA	Tryptophan, threonine, ofloxacin	MCE	The size of Fe_3O_4 NPs and Fe_3O_4@Au NPs were about 8–10 nm and 25–30 nm, and the thickness of the Au shell was 9 nm. Rs were 1.67 (Trp). 1.79 (threonine) and 2.15 (ofloxacin)	83
Fe_3O_4@SiO_2 @PAMAM	BSA	Tryptophan, phenylalanine, histidine	HPLC-PDA	The mean diameter of Fe_3O_4 was 400 nm, thickness silica layer was 60 nm. BSA–PMNPs gave stronger interactions the (−)-enantiomers than the (+)-enantiomers	84
Fe_3O_4@SiO_2 @PAMAM	HSA	Trp, warfarin, ibuprofen	CD and CE	Av diameter of a core–shell structure was 600 nm. HSA–PMSM preferred to interact with the (−)-enantiomers than (+)-enantiomers for (D,L)-Trp and warfarin. In contrast, ibuprofen was the other way around	85
Fe_3O_4/SiO_2	Cationic β-CD	Dansyl (D,L)-valine, dansyl (D,L)-leucine, dansyl (D,L)-phenylalanine	CE	Av particle size was about 580 nm. Cationic-β-CD-modified Fe_3O_4/SiO_2 interacted better with the (L)-enantiomer. Enantiomeric excess for Phe, Leu, and Val are 12.3, 10.0, and 9.6, respectively	73
Fe_3O_4/SiO_2	Maleic anhydride-β-CD (MAH-β-CD)	Trp, Phe, 2-phenylglycine, chlorpheniramin	CE	Av. size of 550 nm. MAH-β-CD-modified Fe_3O_4 microspheres interacted better with (−)-enantiomers than (+)-enantiomers. It was obtained ee of 12.6% and 13.7% for enantioseparation of (D,L)-trp and chlorpheniramine, respectively	74

Table 2 (*Contd.*)

Core/Shell	Chiral selector	Chiral compound(s)	Separation/detection	Remarks	Ref.
Fe_3O_4@PDA	MIP	Tryp, tyrosine, Gly–Phe, ofloxacin	OT-CE	Fe_3O_4@PDA NPs have an average diameter of 146 nm. ~8 nm in thickness of MIP. The resolution factor was about 1.65, 1.76, 3.15, and 2.16 for D,L-Trp, D,L-tyrosine, Gly- D,L-Phe, and racemic ofloxacin, respectively	126
Fe_3O_4	Helical substituted polyacetylene	Alanine	SEM, XRD, CD spectra	(*R*)-PSA-based microspheres give strong interaction to D-ala with an ee of 79%. Whereas (*S*)-PSA-based microspheres is the other way around with the ee of 62%	78
Fe_3O_4	Helical substituted polyacetylene	Alanine	SEM, XRD, CD spectra	After three rounds of enantioselective crystallization, the obtained ee is up to 89%	79
Fe_3O_4/SiO_2	β-CD-epichlorohydrin polymers (β-CD-EP)	Trp	CE	β-CD-EP-modified Fe_3O_4 absorbs more L-Trp. The supernatant ee of D,L-Trp reached up to 44.2% after interaction with 300 mg of β-CDEP-modified Fe_3O_4	127
iFe_3O	Metal–organic frameworks (MOFs) *i.e.* [Zn_2(bdc)(L-lac)(dmf)](DMF), (ZnBLD)	Phenyl methyl sulfoxide, phenyl vinyl sulfoxide, 4-chlorophenyl methyl sulfoxide	HPLC	The best ee was obtained for the separation of phenyl methyl sulfoxide, *e.g.*, 85.2%	128
Fe_3O_4@PNE (polynorepinephrine)	MIP	Tryptophan, valine, threonine, Gly–Phe, ofloxacin, binaphthol	PDMS microchip device	Particle diameter size is 100 nm on average. PNE coats NPs in 6 nm of thickness. For trp, val, thre, ofloxacin, Gly-D,L-Phe, and binaphthol obtained Rs of 1.84, 1.54, 2.17, 3.33, 3.53, and 1.66, respectively	77
Fe_3O_4	Helical substituted polyacetylene	Threonine	SEM, XRD, CD spectra	The complex particles mostly induced L-threonine to form rectangular-shaped crystals with an ee up to 90% after two times of enantioselective crystallization	80
Fe_3O_4@SiO_2	Chiral amino acid ionic liquid, HMDI-EMIMLpro	Cysteine (Cys), arginine (Arg), leucine (Leu), glutamine (Glu), tryptophan (Trp)	Automatic digital polarimeter and centrifugal chiral chromatography	Av diameter of the cluster was 80 nm with average nanoparticles size of about 13 nm. Fe_3O_4@SiO_2@HMDI-EMIMLpro nanospheres preferred to interact with the (+)-enantiomers than that with the (−)-enantiomers cys, arg, and glu. Whereas for Leu and Trp is the other way around	129
Fe_3O_4@SiO_2	Cellulose-2,3-bis(3,5-dimethylphenylcarbamat) (CBDMPC)	Benzoin methyl ether, promethazine hydrochloride, (±)-2-phenoxypropinionic acid, 4-phenyl-1,3-dioxane, DL-*sec*-phenethyl alcohol	Automatic digital polarimeter	The mean diameter of Fe_3O_4@SiO_2@CBDMPC was 545 ± 20 nm. Fe_3O_4@SiO_2@CBDMPC preferred to interact with the (−)-isomer than the (+)-isomer	130
Fe_3O_4@SiO_2	CBDMPC	Benzoin	Chiral microsphere magnetic chromatography	The mean diameter of the microspheres was 240 ± 20 nm. L-benzoin has a high affinity to the chiral selector. The Rs is 1.5	131

Table 2 (*Contd.*)

Core/Shell	Chiral selector	Chiral compound(s)	Separation/detection	Remarks	Ref.
Fe_3O_4@ZrO_3	Cellulose tris(3,5-dimethylphenylcarbamate) (CDMPC)	Propronolol, alprenolol, pindolol, metoprolol, atenolol, carvedolol, ibuprofen, ketoprofen	Automatic Polarimeter	The average particle size is 340 nm. The synthesized particle preferred to bind with (−)-enantiomer of propronolol, alprenolol, pindolol, metoprolol, and atenolol. It is the other way around for carvedolol, ibuprofen, and ketoprofen	132
Fe_3O_4	Cellulose tris-(4-methylbenzoate) (CTMB)	Ibuprofen	HPLC	Fe_3O_4@CTMB interacted stronger with the (*S*)-enantiomer than the (*R*)-enantiomer of ibuprofen. At the single stage, ee was 4.7%. At four steps, the ee was 26.3%	89
TiO_2@SiO_2	Cellulose tris(3,5-dimethylphenylcarbamate) (CDMPC)	Eight basic indole ring derivatives	HPLC	From eight indole rings compound, at optimized conditions, only two obtained Rs > 1.5. The best Rs up to 2.89 was achieved	90
TiO_2@SiO_2	(CDMPC)	2-Hydroxyl-phenylacetonitrile, α-phenylethanol, matalaxyl, and diclofop-methyl	HPLC	Chromatogram shows qualitatively CSP could separate 2-hydroxyl phenylacetonitrile and α phenylethanol well. Rs matalaxyl up to 3.75. RS diclofopmethyl up to 1.67	91
SCMNSs (silica-coated magnetite nanospheres)	Bovine hemoglobin	Tryptophan	Spectrofluorometric	Av size of nanospheres (Hb-SCMNSs) was about 94 nm, with the thickness of the coating layer being about 29 nm. Hb-SCMNSs effectively adsorb the (L)-trp in the presence of (D)-Trp	86
SCMNSs	Tryptophan	Naproxen and phenylglycine	Resonance light scatterings measurements	Av diameter of Try-SCMNSs was 130 nm. –MNSs are very sensitive towards + NAP and +PHY enantiomers and, on the other way around	88
MNPs, *i.e.*, hydroxyl group-modified superparamagnetic nanospheres	MIP	Ofloxacin	Microfluidic channel	The Av diameter of nanoparticles was 200 nm. The obtained Rs of ofloxacin was 1.46	133
Mesoporous silica-coated MNPs (MSMNPs)	Teicoplanin	(D,L)-Tryptophan, (D,L)-phenylalanine, (D,L)-mandelic acid, (D,L)-1-phenyl-1,2-ethanediol, *N*-benzoyl-(D,L)-alanine	CE	Av diameter was about 600 nm, and the mean pore size was 3.9 nm. Optical purity for Trp, Phe, MA, Phe-e, and benzoyl-ala was obtained at 35.4, 27.8, 8.0, 13.7, and 34.2%, respectively	87
MSNPs	(*R*)- and (*S*)-*N*-(2,2-dimethyl-4-pentanoyl)-proline-3,5-dimethylanilide	*N*-(3,5-Dinitrobenzoyl) alanine, valine and leucine, *N*-propylamide	HPLC-UV	Av size MSNPs: 300 nm. (*S*)-enantiomer was preferred to adsorb by MSNPs/(*S*)-CS. The ee using MSNPs/(*S*)-CS was 38.2% in (*S*) for ala, 29.3% in (*S*) for Val, and 13.8% in (*S*) for Leu. Whereas for propylamide, the Rs using MSNPs/(*S*)-CS was 68.1% ee in (*S*) and using NMSPs/(*R*)-CS 80.1% ee in (*R*)	134

Table 3 Carbon-based nanoparticles in the identification and separation of enantiomers

Core/Shell	Chiral selector	Chiral compound(s)	Separation/detection	Remarks	Ref.
Multi-wall CNTs (MWCNTs)	HP-β-CD	Clenbuterol	TLC	Diameter: 10–20 nm; length: 2–20 m. the RF value is 5.27 > pure HP-β-CD impregnated TLC (RF = 3.35)	99
Single-walled nanotubes (SWCNTs)	Polymer mono-lithic backbone	Twelve classes of pharmaceutical racemates	HPLC	Av diameter: ∼1 nm; length, 1–10 nm. RS range from 1.34–2.87	100
CNTs	Pyrenyl derivative coated CNT monolithic column	Ten amino acids	HPLC	Av. diameter: 1 nm; length: <10 nm, Rs varied from 0.94–1.58	101
Magnetic MWCNT	(L)-Threonine	Mandelic acid (MA)	Automatic digital polarimeter and HPLC	The synthesized particle preferred interacting with the (D)-MA than the (L)-MA. The obtained optical purity was up to 54% for (D)-MA	135
SWCNTs and MWCNTs	β-CD	Sulconazole, ketoconazole, citalopram hydrobromide, and nefopam hydrochloric	EKC	The outer diameter of SWCNTs and MWCNTs were 1–2 nm; and 10–20 nm, respectively. Rs up to 3.1 for SUL and 4.5 for KET. 2.9 for CIT and 1.4 for NEF	102
SWCNTs and MWCNTs	Single-walled nanotubes surfactant-coated carbon nanotubes	(±)-Ephedrine, (±)-norephedrine and (±)-*N*-methylephedrine	EKC	Diameters and lengths of SWCNTs were within 0.7–1.2 nm and 2–20 μm, while MWCNTs were within 6–20 mm and 1–5 μm, respectively. Rs for norephedrine and ephedrine were 1.49 ($\alpha = 1.04$) and 1.35 ($\alpha = 1.03$), respectively	103
MWCNTs	β-CD	Clenbuterol	CE	Interlayer spacing of 3.4 Å; typical diameter of 10–20 nm. Selectivity (α) up to 1.035	104
Ionic liquid dispersed MWCNTs	Chondroitin sulfate E	Amlodipine (AML), laudanosine (LAU), nefopam (NEF), citalopram (CIT), and propranolol (PRO)	CE	The outer diameters and lengths of MWCNT in between 10–20 nm and 5–30 nm, respectively. Rs 3.03, 2.01, 1.7, 0.95, and 0.98 were obtained for AML, LAU, NEF, CIT, and PRO, respectively	105
SWCNTs	BSA	Trp	Microchip electrophoresis	At 32 cm of microchip length, Trp enantiomers separation was reached within 70 s with Rs of 1.35	136
MWCNTs	BSA	Ketoprofen, ibuprofen, uniconazole, and hesperidin	CEC	Resolutions of 24.20, 12.81, 1.50, and 1.85 for ketoprofen, ibuprofen, uniconazole, and hesperidin, respectively	137
Graphene	(D)-(−)-Tartaric acid (DTA)	Propranolol and ofloxacin	TLC	The thickness of the graphene nanosheet is 2–3 nm. Obtained Rs is 2.77 for ofloxacin and 6.8 for propranolol	108
Graphene	Graphene nanosheets with tetracyanoethylene oxide and (*S*)-(+)-2-pyrrolidineme OH	Ibuprofen and thalidomide	HPLC	The best selectivity was achieved up to 12.5 for ibuprofen, whereas for thalidomide $\alpha = 17.5$	110
Graphene oxide (GO)	Methyl β-CD	Naproxen, warfarin, and pranoprofen	CE	In the bare capillary column was no resolution. Rs in GO-polymer-coated capillary column improved to 1.56, 1.89, and 1.51 for naproxen, warfarin, and pranoprofen, respectively	111
GO	HAS or pepsin	Phenylalanine, azelastine, warfarin, ibuprofen, trp, salbutamol, chlortrimeton, propranolol, and nefopam	CEC	The presence of GO improved all enantiomeric separation of nine analytes compared to the column without GO, *e.g.*, ibuprofen could reach Rs of 3.5 in the column with GO, whereas there was no separation in the column without GO	107
Polydopamine–graphene oxide (PDA/GO)	BSA	Trp, threonine, and dipeptide	CEC	Rs of Trp, threonine, and dipeptide were about 1.78, 1.76, and 1.74, respectively. The RS is improved compared with the native microchip (without PDA/GO coating)	138

Table 3 (*Contd.*)

Core/Shell	Chiral selector	Chiral compound(s)	Separation/detection	Remarks	Ref.
GO	—	Ephedrine-pseudoephedrin (E-PE) and β-methylphenethylamine (β-Me-PEA)	CE	Rs of E-PE were between 0.57–0.92 and baseline resolution for β-Me-PEA	112
$GO@SiO_2$	Cellulose (3,5-dimethylphenylcarbamate)	Ibuprofen, *trans*-stilbene oxide, (*R*,*S*)-equol, benzoin, praziquantel, propranolol, ketoconazole, quinidine, 2-phenylcyclohexanone	HPLC	RS for all analytes ranges from 1.48–4.83	106
MGO@PNG poly(*N*-isopropylacrylamide-*co*-glycidyl methacrylate)	β-CD	(D,L)-Trp	HPLC	Diameter ~80 nm, thickness 8 nm. At 25 °C, enantioseparation of (D,L)-Trp by the β-CD-combined MGO@PNG-CD reached equilibrium with ee up to 100%	139

their surfaces with silica and carboxymethyl-β-cyclodextrin (CMCD).[71] A chromatographic method was employed to quantify the separation of enantiomers from a racemic mixture, measuring the enantiomeric excess. The MNPs exhibited selective adsorption of (L)-enantiomers of (D,L)-tryptophan, (D,L)-phenylalanine, and (D,L)-tyrosin from the racemic mixture, resulting in ee of 94%, 73%, and 58%, respectively.[71] Simplified adsorption mechanism of Trp onto Fe_3O_4/SiO_2/CMCD MNPs schematically illustrated at Fig. 7.

The use of mNPs functionalized with a helical polymer give high ee up to 90% in the enantioseparation of threonine enantiomers. The core of the microspheres comprises magnetic Fe_3O_4 nanoparticles (NPs) coated with a shell made of helical polyacetylene, resulting in magnetic Fe_3O_4@PA core/shell microspheres. The presence of the microspheres led to the preferential formation of rectangular-shaped crystals of (L)-threonine. Beside give a good ee, it was reported that the microspheres demonstrated convenient recyclability using an external magnetic field.[80] Highlighting their promising potential in various chiral-related applications.

Studies of the use of metal oxide nanoparticles for enantioseparation, including the shell (coating materials), employed chiral selector, analytes, detection, and remarks on the performance of the reported NPs for enantioselective separations are provided in Table 2. Several combinations of metal oxide-based nanoparticles and chiral selectors have been studied. However, there are still difficulties that need to be addressed to get full enantioseparation in a single step.

3.3 Carbon-based nanoparticles

The study of carbon-based nanomaterials has increased quickly over the past decade. Carbon-based nanomaterials are being employed as absorbents[92] and essential components in preconcentration,[93] extractions, or separation process,[93] primarily because of their exceptional durability, robust chemical stability, remarkable flexibility, and excellent thermal conductivity. The variant of carbon-based nanomaterials like CNTs, graphenes, and graphene oxides (GOs) have been introduced to the field of enantiomeric separation.[12,34] Some applications and fabrication concerning CNTs, graphenes, and graphene oxide nanomaterials in this field are presented in the following section.

3.3.1 Carbon nanotube-based nanomaterials. Carbon nanotubes (CNTs) are carbon allotropes that have a cylindrical shape and possess unique characteristics, which offer significant potential for their use in a broad range of industrial applications.[92] Based on the number of tubes present within their structures, CNTs are classified into two, *e.g.*, single-walled CNTs (SWCNTs) and multi-walled CNTs (MWCNTs).[92] Several methods for producing CNTs in significant quantities include the carbon arc-discharge technique, laser ablation, sonochemical or hydrothermal methods, electrolysis, and chemical vapor deposition. Carbon arc discharge and laser ablation were the initial techniques employed to synthesize SWCNTs in large quantities, while they are also suitable for MWCNT synthesis.[92] CNTs are gaining increasing attention as potential candidates

for application in separating various compounds, primarily because of their remarkable physicochemical characteristics and significant chemically reactive surface region.[93–97] CNTs have the potential to improve the pace, selectivity, durability, and efficacy of chiral chromatography, thereby facilitating enantiomeric separation.[12,98]

The application of CNT in thin-layer chromatography (TLC) for enantioseparation has been reported.[99] The surface of MWCNT is modified with a chiral selector HP-β-CD for the separation of clenbuterol enantiomers.[99] The use of MWCNT-HP-β-CD impregnated TLC in the separation of clenbuterol enantiomers reached a retention factor of up to 5.27, while the obtained RF using HP-β-CD impregnated TLC is 3.35.[99] It is clear that the use of CNT improved the separation of clenbuterol enantiomers.

In chiral HPLC, the use of CNT has been successfully investigated for the enantiomeric separation of several chiral compounds. Ahmed *et al.* developed a chiral stationary phase (CSP) by incorporating a small quantity of SWCNTs into polymer monolithic backbones.[100] The produced CSP showed effective enantioselectivity for the separation of twelve types of pharmaceutical racemates with an Rs value ranging from 1.34 to 2.87.[100] The enantiomeric separations of ten amino acids racemates have been successfully achieved by using SWCNTs combined with pyrenyl derivative as chiral stationary phases (CSPs) with Rs value ranging from 0.94–1.58.[101]

CNTs have been applied for enantiomeric separation in electrokinetic chromatography (EKC) and capillary electrophoresis (CE) systems as pseudostationary phases. In combination with dextrin, CNTs have been used for the enantioseparation of several chiral compounds, namely sulconazole, ketoconazole, citalopram, and neofam hydrochloric.[102] The addition of CNTs to the buffer resulted in an enhancement in the resolution of sulconazole and ketoconazole, with the values increasing from 2.78 to 3.20 and 3.47 to 4.52, respectively, as compared to the buffer without CNTs.[102] Combined with a surfactant (as a chiral selector), SWCNTs and MWCNTs have been used for the enantioseparation of ephedrine, norephedrine, and *N*-methylephederine.[103] The use of MWCNTs-modified-B-CD for enantioseparation of Clenbuterol reported by Na *et al.*[104] Zhang *et al.* investigated the use of CNTs for enantioseparation of several chiral drugs. Interestingly, in their study CNTs are coated with ionic liquid before being applied to the background electrolyte consisting of chondroitin sulfate *E* as chiral selector.[105] From all mentioned studies about the use of CNTs, all enantioseparation of the analytes shows much better than the separation without CNTs.[103–105] Reported studies of the use of SWCNTs and MWCNTs for enantioseparation are summarized in Table 3.

In general, the use of nanoparticles improved the separation. According to Hua *et al.*[102] and Zhang *et al.*,[105] the use of CNTs improved the resolutions compared to bare or pure chiral selectors because of the improved shapes of the peaks. That can be clarified by the fact that the attachment of the analytes to the capillary wall was prevented.[102] In addition, nanoparticles offer a significant surface area for the adsorption of chiral selectors, leading to improved contact and interaction between chiral selectors and analytes.

3.3.2 Graphene and graphene oxide-based nanomaterials. Graphene is one of the attractive nanomaterials for a wide field of applications. Graphene often requires chemical modification as graphene oxide (GO) in getting its exceptional physical and chemical properties before being used to create composites and subsequently reduced.[106] Graphene and graphene oxide (GO) nanomaterials are highly potential candidates for making innovative stationary phases in various separations.[12,34,107]

In the enantiomeric separation of chiral compounds, Graphene and GO have been reported in several publications. For instance, incorporating graphene as an adjustable additive in the stationary phase enhanced the chiral separation performance of racemic propranolol in the chiral selector (CS) impregnated TLC.[108] The Rs of propranolol from 3.5 with pure CS-impregnated TLC[109] improved to 6.8 with the addition of graphene in the stationary phase.[108] Another study reported a novel CSP class based on graphene that is chemically resistant, adaptable, and affordable for separating enantiomers using liquid chromatography.[110] The enantiomeric separation of ibuprofen and thalidomide racemates was achieved using

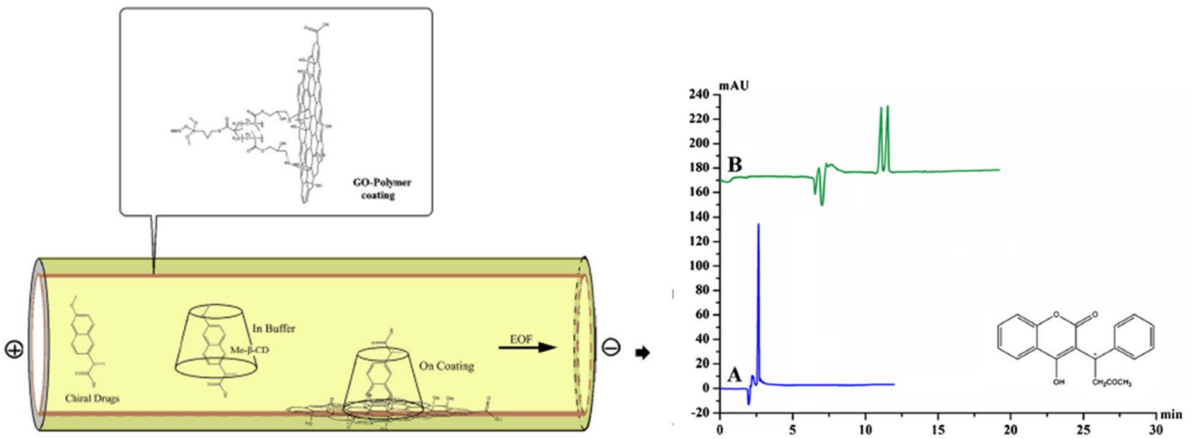

Fig. 8 The scheme of separation in a bare and coated capillary and typical electropherograms of the chiral separation of Warfarin in bare (A) and coated capillary (B). Modified with permission from ref. 111 (© Springer-Verlag Wien 2016).

Table 4 Other Nanomaterials in identification and separation of enantiomers

Core/shell	Chiral selector	Chiral compound(s)	Separation/detection	Remarks	Ref.
Poly-ethylene dimethacrylate–*N*-methacryloyl-L-histidine methyl ester (EGDMA–MAH) NP	(L)-Histidine	Ofloxacin	CE	Average (Av) size of NP ~111.5 nm. The separation factor up to 2.9 was successfully achieved	140
Mesoporous silica NP	Cellulose tris(3,5-dimethylphenylcarbamate) (CDMPC)	Benzoin, indapamine, Tröger's base, praziquantel, DDBD, OHBN, warfarin, tetrahydropalmatine and pindolol	CEC	The particle and pore size was 600 nm and 300 nm, respectively. No Rs for paraziquantel was achieved. For other racemates, the Rs range from 1.14 to 5.28	141
Zeolite imidazolate nanocrystal	BSA	Salbutamol sulfate	CE	Compared to bare columns with no separation, a good separation was achieved using BSA@ZIF-8-OT columns	142
Metal–organic framework (MOF)	Chiral bridging ligand [{Cu(sala)$_n$] (H2sala = *N*-(2-hydroxybenzyl)-L-alanine)	Citronellal, Camphor, Ala, Leu, Val, Isoleu, 1-phe-1,2-ethandiol, phenylsuccinic acid, and 1-phe-ethanol	GC	Separation factor range (α) from 1.01–1.33	143
Polystyrene NP (PSNPs)	Hydroxypropyl-β-CD (HP-β-CD)	Propanolol	CE	Av diameter of 15 ± 5 nm. The separation with PS improved to 0.92 from 0.6 (without PS at BGE)	122
Mesoporous silica NP	CM-β-CD	Ephedrine (EPHE) and chlorpheniramine (CHLORPHE)	CE	Sz approximately 120 nm. At optimum conditions, Rs improved from 0.86 to 1.05 (ephedrine) and from 0.88 to 1.12 (chlorpheniramine)	144
G3.0-PMMPs	(L)-Val	Dansy (D,L)-phe	CE	L-Val@G3.0-PMMPs mostly adsorbed dansyl (L)-phe. The obtained ee was 20.1%	145
poly(glycidyl methacrylate) (PGMA) NPs	Ethanediamine-β-CD	Propranolol (prop) metoprolol (metopro) amlodipine (amlo)	CEC	Best resolutions were obtained at 1.27, 1.01, and 2.93 for prop, metopro, and amlo, respectively	146
SiO_2@PDA	BSA	Prop and trp	CE	Particle size ~150 nm. In five adsorption steps, ee of Trp and prop are 14.50% and 11.71%, respectively. When starting racemic solution is 75% ee, after adsorption with SiO_2@PDA@BSA gave 100% ee (solution is purified)	121
Silica	PEO113-*b*-((D,L)-GluA)10	Val	Circular dichroism (CD) and polarimetry	The pore sizes of the CMS sphere were within 2–3 nm. The ee of separation was 50%	118
Mesoporous silica	The L-forms of the target analytes	Pro, Ile, *trans*-4hyp, pipecolic acid, Val, Leu, Phg	HPLC-ESI-MS	Obtained pore sizes in the range of 2.8–3.3 nm. Separation factor, α, for Pro, Ile, *trans*-4hyp, pipecolic acid, Val, Leu, Phg were obtained 6.26, 1.30, 0.7, 1.5, 1.09, 1.12, and 1.15 respectively	117
Mesoporous silica	(L)-Phenylalanine	(D,L)-Phenylalanine, (D,L)-ala and (D,L)-lysine	CD spectra	The pore sizes were within 2.3–2.5 nm. The synthesized materials gave stronger adsorption for (L)-phenylalanine with a capacity of up to 3.24	120
Mesoporous silica nanospheres	Chiral anion surfactant (*N*-palmitoyl-L-phenylalanine)	Alanine	CD spectroscopy	The particle size and pore diameters were within 190 nm-210 nm and 3 nm-4 nm, respectively. Chiral selectivity factor of 3.15	114
Mesoporous silica	(D)- or (L)-proline	Proline	CD	Pore sizes in the range of 2.6–3.2 nm. (D,L)-racemate separation factor ($\alpha_{D/L}$) is 3.2	116

Table 4 (*Contd.*)

Core/shell	Chiral selector	Chiral compound(s)	Separation/detection	Remarks	Ref.
Mesoporous silica	Aspartic acid block copolymer	Valine	CD and optical polarimetry	CMS with a pore size of 3–5 nm. chiral selectivity factor of 7.52	119
Mesoporous silica	Guanosine monophosphate (NGM-1) and folic acid (NFM-1)	Valine	CD	cNFM-1 preferred to adsorb L-valine than D-valine with an adsorption ratio of 2.6, while cNGM-1 preferred to adsorb D-valine than D-valine with an adsorption ratio of 4	147
Mesoporous silica	Copolymers of poly(ethylene oxide) (PEO) and chiral (D,L)-phenylalanine – glutamic acid [PEO-β-(L,D)-GluA) and blocks of chiral (L,D)-phenylalanine [PEO-b-((L,D)-Phe)	Valine	CD	The pore's diameter was between 3.5–3.7 nm. The synthesized nanoparticles mostly adsorb L-valine; the obtained ee was 54%	115

graphene nanosheets that were modified with tetracyanoethylene oxide (TCNEO) and (*S*)-(+)-2-pyrrolidinemethanol. The modified graphene gave high enantioselectivity for ibuprofen and thalidomide, *i.e.*, up to 12.5 and 17.5, respectively.

The utilization of GO in enantiomeric separations is used as a coating material for capillary in CE (and CE derivatized) systems. The GO-coated capillary column has been used for the enantioseparation of naproxen, warfarin, and pranoprofen.[111] In combination with methyl-β-CD as a chiral selector, the coated capillary column gave the Rs of naproxen, warfarin, and pranoprofen are 1.56, 1.89, and 1.51, respectively.[111] While in the bare capillary column (without GO coating), no separation was achieved, although using a similar chiral selector (methyl-β-CD).[111] The scheme of separation in a bare and coated capillary and typical electropherograms of the chiral separation of Warfarin in bare and coated capillary are shown in Fig. 8. The presence of graphene oxide (GO) can potentially impede the entry of analytes into the cavity of Me-β-CD from the wider rim. This alteration in the chiral recognition process of Me-β-CD could ultimately lead to enhanced enantioseparation performances.

Notably, a capillary coated with graphene oxide (GO) was capable of separating ephedrine-pseudoephedrine (E-PE) isomers and β-methylphenethylamine (β-Me-PEA) isomers into their respective enantiomers even in the absence of a known chiral selector.[112] Although the obtained resolution for E-PE is still low, *i.e.*, max 0.98, the enantioseparation of β-Me-PEA reached a baseline resolution.[112]

Studies regarding the use of graphene dan GO for the enantioseparation of various compounds are shown in Table 3. Generally, the presence of graphene and GO improved the interaction and contact between analytes and chiral selectors, resulting in enhanced resolution. However, the studies reported by Ye *et al.*[112] show that GO can also act as a chiral selector so that even though there is no chiral selector, the presence of GO chiral separation gave resolution for the separation of E-PE and β-Me-PEA enantiomer. That can be explained by the unique characteristic of GO under an electric field (CE system) may offer chiral recognition sites, with electrostatic attraction and hydrogen bonding as the driving forces to interact better with one of the enantiomers.[112]

3.4 Other nanomaterials

Other nanomaterials in combination with a chiral selector have been used for the enantioseparation without the presence of metallic-, metal oxide-, and carbon-based nanomaterial. Some of the published reports regarding the use of other nanomaterials or nanoparticles for enantioselective separation are shown in Table 4. Several studies mostly used mesoporous silica nanoparticles (NPs) as core or shell to be modified with a chiral selector for enantioseparation of a chiral compound. Besides, polymer nanoparticles such as derivatized poly-ethylene NP, polystyrene NP, poly(glycidilmetacrylate), and zeolite have successfully achieved for enantioseparation of several chiral compounds.

Chiral mesoporous silica (CMS) nanoparticles have a broad application in separating chiral compounds with high

selectivity and adsorption capability due to their unique chiral-structural features.[113] The reported studies of the use of CMS mostly used for enantioseparation of amino acids compounds such as alanine,[114,115] proline,[116,117] valine,[115,118,119] and phenylalanine.[120] In general, CMS is synthesized by combining tetraethyl orthosilicate and other silica sources with the presence of template molecule, *i.e.*, enantiopure (D- or L-form) of the analyte. From several reports here, the obtained selectivity of absorption also represents the chiral selectivity factor, ranging from 3 to 7.5 (summarized in Table 4).

Another exciting work has been reported by Li and co-workers.[121] This group separated propranolol and tryptophan enantiomers by utilizing silica nanoparticles functionalized with bovine serum albumin as adsorbents.[121] It has been reported that multistep adsorption is needed to enhance the ee. At multistep, adsorption starts from a high initial ee (75.55%) after adsorption, and then the ee of the resulting solution is up to almost 100%.[121] Besides silica nanoparticles, polystyrene (PS) nanoparticles have been successfully employed to manipulate chiral selectivity.[122] PS nanoparticles have been used for chiral propranolol analysis by capillary electrophoresis. PS was dispersed into the background solutions containing HP-β-CD as a chiral selector.[122] PS nanoparticles play a role in the enantioseparation, *e.g.*, improving the peak shape of the separation.[122]

In general, nanoparticles offer the ability to manipulate aggregation, colloidal assembly, and molecular adsorption by providing a significant surface area, leading to improved contact and interaction between chiral selectors and analytes. These enabling a valuable approach to comprehending enantioselective processes by describing chemical dynamics on particle surfaces.

4 Summary and future works

The use of surface-modified nanomaterials, including nanoparticles, nanotubes, and nanoporous, holds great potential in the enantioselective recognition and separation of various chiral compounds. From reviewed papers, the use of nanomaterials modified with chiral selectors has increased the selectivity, sensitivity, and efficiency of enantioselective recognition and separation. Commonly techniques like HPLC, GC, and CE, which are employed for detection and analysis chiral compound concentration, tend to be expensive, time-consuming, and labor-intensive. Additionally, these methods generate significant amounts of solvent waste. Surface-modified nanomaterials, specifically from metal-based nanomaterials group, offer an entirely detection methods that rapidly and accurately distinguish enantiomers. Several reports of the use of nanomaterials in the enantioselective separation show that the enantiomeric excess (ee) still needs to be increased in terms of getting a complete separation or purification of the racemic solution. The use of multistage separation and investigation of the other combination of nanomaterials with a chiral selector to get a high ee is recommended. As demonstrated by Li *et al.*,[121] Fu *et al.*,[81] and Zhang *et al.*,[79] the use of multistep separation has improved the ee. Furthermore, the use of nanoparticles in detection and or separation is as a modifier and supporting material to the chiral selector in existing methods. It is reasonable that enantiomer detection and separation still have challenges in the broad range of applications, the cost associated with the selector, and the productivity of the separation. Therefore, a more adaptable, efficient, and cost-effective technique for enantioseparation still needs to be explored. According to the principle of sustainable and green chemistry, recycling valuable functional nanoparticles is highly recommended, besides the need for efficient and effective separation. The investigation of the other combination of nanomaterials with a chiral selector for efficient and effective enantioselective separation will be further studied in the near future, especially for the enantioselective separation of chiral drugs.

Author contributions

Susanti; Writing original draft preparation and editing. Asep Riswoko.; Writing, review, and editing. Joddy Arya Laksmono; review and supervision. Galuh Widiyarti; review. Dadan Hermawan; review.

Conflicts of interest

Authors declare no conflict of interest.

Acknowledgements

This work was supported by The Deputy of Human Resources for Science and Technology-National Research and Innovation Agency (BRIN) (No. 151/II/HK/2022) and the Research Organization for Nanotechnology and Material (ORNM)-BRIN (No. B-613/III.10/PR.03.06/2/2023). Thank you to the staff of BRIN Library for the proofreading and A. P. Kristijarti for assisting in the process of acquiring relevant literature.

References

1 B. Waldeck, *Pharmacol. Toxicol.*, 2003, **93**, 203–210.
2 A. P. Jiří and Z. Dvořák, *J. Appl. Biomed.*, 2004, 95–100.
3 S. J. Mohan, E. C. Mohan and M. R. Yamsani, *Int. J. Pharmaceut. Sci. Nanotechnol.*, 2009, **1**, 309–316.
4 H. U. Blaser, *Rendiconti Lincei.*, 2013, **24**, 213–216.
5 E. Zor, *Talanta*, 2018, **184**, 149–155.
6 I. Ali and H. Y. Aboul-Enein, *Chiral Pollutants: Distribution, Toxicity, and Analysis by Chromatography and Capillary Electrophoresis*, 2004.
7 W. Liu and M. Tang, in *Herbicides-Mechanisms and Mode of Action*, ed. M. N. Hasaneen, InTech Europe, Rijeka, 2011.
8 C. V. Bui, T. Rosenau and H. Hettegger, *Molecules*, 2021, **26**, 4322.
9 L. Friedman and J. G. Miller, *Science*, 2013, **172**, 1044–1046.
10 M. Steensma, N. J. Kuipers, A. B. de Haan and G. Kwant, *Chirality*, 2006, **18**, 314–328.
11 D. Haan, in *Ion Exchange and Solvent Extraction*, ed. J. A. Marcus, Y. SenGupta and K. Arup Marinsky, Marcel Dekker Inc, New York, 2002, p. 255.

12 A. Gogoi, N. Mazumder, S. Konwer, H. Ranawat, N. T. Chen and G. Y. Zhuo, *Molecules*, 2019, **24**, 1007.
13 H.-U. Blaser and M. Studer, *Chirality*, 1999, **464**, 459–464.
14 N. S. Bowman, G. T. McCloud and G. K. Schweitzer, *J. Am. Chem. Soc.*, 1968, **90**, 3848–3852.
15 A. N. Collins, G. N. Sheldrake and J. Crosby, *Chirality in Industry II: Developments in the Commercial Manufacture and Applications of Optically Active Compounds*, John Wiley & Sons, 1997.
16 N. M. Maier, P. Franco and W. Lindner, *J. Chromatogr. A*, 2001, **906**, 3–33.
17 G. K. Schweitzer, I. R. Supernaw and N. S. Bowman, *J. Inorg. Nucl. Chem.*, 1968, **30**, 1885–1890.
18 S. J. Romano, K. H. Wells, H. L. Rothbart and W. Rrieman III, *Talanta*, 1969, **16**, 581–590.
19 K. Tang, J. Yi, K. Huang and G. Zhang, *Chirality*, 2009, **21**, 390–395.
20 H. Lorenz and A. Seidel-Morgenstern, *Angew. Chem., Int. Ed.*, 2014, **53**, 1218–1250.
21 M. Schulte and J. Strube, *J. Chromatogr. A*, 2001, **906**, 399–416.
22 A. Seidel-Morgenstern, L. C. Keßler and M. Kaspereit, *Chem. Eng. Technol.*, 2008, **31**, 826–837.
23 A. Rajendran, G. Paredes and M. Mazzotti, *J. Chromatogr. A*, 2009, **1216**, 709–738.
24 F. Tassinari, J. Steidel, S. Paltiel, C. Fontanesi, M. Lahav, Y. Paltiel and R. Naaman, *Chem. Sci.*, 2019, **10**, 5246–5250.
25 H. Lorenz, D. Polenske and A. Seidel-Morgenstern, *Chirality*, 2006, **18**, 828–840.
26 H. Lorenz, F. Capla, D. Polenske, M. P. Elsner and A. Seidel-Morgenstern, *J. Chem. Eng. Process.*, 2007, **42**, 5–16.
27 T. Gumí, C. Palet, Q. Ferreira, R. M. C. Viegas, J. G. Crespo and I. M. Coelhoso, *Sep. Sci. Technol.*, 2005, **40**, 773–789.
28 P. J. Pickering and J. B. Chaudhuri, *J. Membr. Sci*, 1997, **127**, 115–130.
29 Z. Wang, C. Cai, Y. Lin, Y. Bian, H. Guo and X. Chen, *Sep. Purif. Technol.*, 2011, **79**, 63–71.
30 B. Schuur, *Enantioselective liquid-liquid extraction in centrifugal contactor separators*, University Groningen, Groningen, 2008.
31 S. Susanti, T. G. Meinds, E. B. Pinxterhuis, B. Schuur, J. G. de Vries, B. L. Feringa, J. G. M. Winkelman, J. Yue and H. J. Heeres, *Green Chem.*, 2017, **19**, 4334–4343.
32 B. J. V. Verkuijl, *Chiral separation by enantioselective liquid-liquid extraction: from novel systems to continuous multistage processes*, 2009.
33 E. B. Pinxterhuis, J. B. Gualtierotti, H. J. Heeres, J. G. De Vries and B. L. Feringa, *Chem. Sci.*, 2017, **8**, 6409–6418.
34 H. Y. Aboul-Enein, N. Bounoua, M. Rebizi and H. Wagdy, *Chirality*, 2021, **33**, 196–208.
35 X. Deng, W. Li, G. Ding, T. Xue and X. Chen, *Separ. Purif. Rev.*, 2017, **48**, 14–29.
36 W. H. Pirkle and T. C. Pochapsky, *Chem. Rev.*, 1989, **89**, 347–362.
37 X. X. Zhang, J. S. Bradshaw and R. M. Izatt, *Enantiomeric Recognition of Amine Compounds by Chiral Macrocyclic Receptors*, 1997.
38 X. Deng, W. Li, Y. Wang and G. Ding, *TrAC, Trends Anal. Chem.*, 2020, **124**, 1–15.
39 D. R. Boverhof, C. M. Bramante, J. H. Butala, S. F. Clancy, W. M. Lafranconi, J. West and S. C. Gordon, *Regul. Toxicol. Pharmacol.*, 2015, **73**, 137–150.
40 H. F. Krug and P. Wick, *Angew. Chem., Int. Ed.*, 2011, **50**, 1260–1278.
41 T. A. Saleh and V. K. Gupta, *Nanomater. Polym. Membr.*, 2016, 83–133.
42 M. Vassal, S. Rebelo and M. de L. Pereira, *Int. J. Mol. Sci.*, 2021, **22**, 1–35.
43 O. V Salata, *J. Nanobiotechnol.*, 2004, **2**, 1–6.
44 M. Sun, X. Wang, X. Guo, L. Xu, H. Kuang and C. Xu, *Chem. Sci.*, 2022, **13**, 3069–3081.
45 J. Hernández-Borges, *Magnetic nanoparticles for solid-phase extraction*, LCGC Europe, 2016, vol. 29, pp. 180–193.
46 N. Baig, I. Kammakakam, W. Falath and I. Kammakakam, *Mater. Adv.*, 2021, **2**, 1821–1871.
47 L. Zhang, Q. Jin and M. Liu, *Chem. Asian J.*, 2016, **11**, 2642–2649.
48 M. Shah, V. D. Badwaik and R. Dakshinamurthy, *J. Nanosci. Nanotechnol.*, 2014, **14**, 344–362.
49 M. Shah, V. Badwaik, Y. Kherde, H. K. Waghwani, T. Modi, Z. P. Aguilar, H. Rodgers, W. Hamilton, T. Marutharaj, C. Webb, M. B. Lawrenz and R. Dakshinamurthy, *Front. Biosci.*, 2014, **19**, 1320–1344.
50 F. Schulz, S. Tober and H. Lange, *Langmuir*, 2017, **33**, 14437–14444.
51 N. Shukla, M. A. Bartel and A. J. Gellman, *J. Am. Chem. Soc.*, 2010, **132**, 8575–8580.
52 F. Keshvari, M. Bahram and A. A. Farshid, *Anal. Methods*, 2015, **7**, 4560–4567.
53 L. Zhang, C. Xu, G. Song and B. Li, *RSC Adv.*, 2015, **5**, 27003–27008.
54 N. Shukla, D. Yang and A. J. Gellman, *Surf. Sci.*, 2016, **648**, 29–34.
55 H. Su, Q. Zheng and H. Li, *J. Mater. Chem.*, 2012, **22**, 6546–6548.
56 P. Gaviña, M. Parra, S. Gil, A. M. Costero, P. Gaviña, M. Parra, S. Gil and A. M. Costero, in *Gold Nanoparticles - Reaching New Heights*, IntechOpen, 2018, pp. 1–15.
57 L. Zhang, C. Xu, C. Liu and B. Li, *Anal. Chim. Acta*, 2014, **809**, 123–127.
58 F.-K. Liu, G.-T. Wei and F.-C. Cheng, *J. Chin. Chem. Soc.*, 2003, **50**, 931–937.
59 R. Huang, D. Wang, S. Liu, L. Guo, F. Wang, Z. Lin, B. Qiu and G. Chen, *Chirality*, 2013, **25**, 751–756.
60 C. Liu, J. Zhang, X. Zhang, L. Zhao and S. Li, *Microchim. Acta*, 2018, **185**, 1–7.
61 Z. Feng, Y. Yang, G. Xu, Y. Du and X. Sun, *Electrophoresis*, 2020, **41**, 1060–1066.
62 L. Yang, C. Chen, X. Liu, J. Shi, G. Wang, L. Zhu, L. Guo, J. D. Glennon, N. M. Scully and B. E. Doherty, *Electrophoresis*, 2010, **31**, 1697–1705.
63 M. Jafari, J. Tashkhourian and G. Absalan, *Talanta*, 2018, **178**, 870–878.

64 S. H. Choi, H. J. Noh and K. P. Lee, *Bull. Korean Chem. Soc.*, 2005, **26**, 1549–1554.
65 M. Zhang and B. C. Ye, *Anal. Chem.*, 2011, **83**, 1504–1509.
66 Y. Li, N. Zhu, Y. Ma, Q. Li and P. Li, *Anal. Bioanal. Chem.*, 2017, **410**, 441–449.
67 E. Öztürk Er, G. Dalgıç Bozyiğit, Ç. Büyükpınar and S. Bakırdere, *Crit. Rev. Anal. Chem.*, 2022, **52**, 231–249.
68 X. Chen, J. Rao, J. Wang, J. J. Gooding, G. Zou and Q. Zhang, *Chem. Commun.*, 2011, **47**, 10317–10319.
69 S. Ghosh, A. Z. M. Badruddoza, M. S. Uddin and K. Hidajat, *J. Colloid Interface Sci.*, 2011, **354**, 483–492.
70 R. P. Liang, C. M. Liu, X. Y. Meng, J. W. Wang and J. D. Qiu, *J. Chromatogr. A*, 2012, **1266**, 95–102.
71 S. Ghosh, T. H. Fang, M. S. Uddin and K. Hidajat, *Colloids Surf. B Biointerfaces*, 2013, **105**, 267–277.
72 M. Arslan, S. Sayin and M. Yilmaz, *Tetrahedron: Asymmetry*, 2013, **24**, 982–989.
73 J. Wu, P. Su, D. Guo, J. Huang and Y. Yang, *New J. Chem.*, 2014, **38**, 3630–3636.
74 J. Huang, P. Su, J. Wu and Y. Yang, *RSC Adv.*, 2014, **4**, 58514–58521.
75 J. Huang, P. Su, B. Zhao and Y. Yang, *Anal. Methods*, 2015, **7**, 2754–2761.
76 D. Liu, L. Zhang, M. Li, W. Yang and J. Deng, *Macromol. Rapid Commun.*, 2012, **33**, 672–677.
77 J. Chen, R. P. Liang, X. N. Wang and J. D. Qiu, *J. Chromatogr. A*, 2015, **1409**, 268–276.
78 H. Chen, L. Li, D. Liu, H. Huang, J. Deng and W. Yang, *RSC Adv.*, 2014, **4**, 63611–63619.
79 H. Zhang, G. Qian, J. Song and J. Deng, *Ind. Eng. Chem. Res.*, 2014, **53**, 17394–17402.
80 H. Chen, J. Zhou and J. Deng, *Polym. Chem.*, 2015, **7**, 125–134.
81 Y. Fu, T. Huang, B. Chen, J. Shen, X. Duan, J. Zhang and W. Li, *Sep. Purif. Technol.*, 2013, **107**, 11–18.
82 R. P. Liang, X. Y. Meng, C. M. Liu, J. W. Wang and J. D. Qiu, *Microfluid. Nanofluidics*, 2013, **16**, 195–206.
83 R. P. Liang, X. N. Wang, L. Wang and J. D. Qiu, *Electrophoresis*, 2014, **35**, 2824–2832.
84 Y. Wang, P. Su, S. Wang, J. Wu, J. Huang and Y. Yang, *J. Mater. Chem. B*, 2013, **1**, 5028–5035.
85 Y. Yang, J. Wu, P. Su, Y. Yang, J. Huang and Y. Wang, *J. Mater. Chem. B*, 2014, **2**, 775–782.
86 H. Bagheri, M. Ahmadi, T. Madrakian and A. Afkhami, *Sens. Actuators, B*, 2015, **221**, 681–687.
87 J. Wu, P. Su, J. Huang, S. Wang and Y. Yang, *J. Colloid Interface Sci.*, 2013, **399**, 107–114.
88 M. Ahmadi, T. Madrakian and A. Afkhami, *Sens. Actuators, B*, 2015, **210**, 439–445.
89 T. Huang, P. Song, L. Jiang, Y. Peng, S. Feng and J. Wang, *Electrophoresis*, 2016, **37**, 2050–2053.
90 J. Ge, W. Zhou, L. Zhao and Y. P. Shi, *Anal. Lett.*, 2007, **40**, 2515–2523.
91 J. Ge, L. Zhao and Y.-P. Shi, *Chin. J. Chem.*, 2008, **26**, 139–142.
92 M. M. Sabzehmeidani, S. Mahnaee, M. Ghaedi, H. Heidari and V. A. L. Roy, *Mater. Adv.*, 2021, **2**, 598–627.
93 A. El-Sheikh, A. H. El-Sheikh and J. A. Sweileh, *Jordan J. Chem.*, 2011, **6**, 1–16.
94 B. S. Harrison and A. Atala, *Biomaterials*, 2007, **28**, 344–353.
95 O. Breuer and U. Sundararaj, *Polym. Compos.*, 2004, **25**, 630–645.
96 J. Song, F. Wang, X. Yang, B. Ning, M. G. Harp, S. H. Culp, S. Hu, P. Huang, L. Nie, J. Chen and X. Chen, *J. Am. Chem. Soc.*, 2016, **138**, 7005–7015.
97 N. Baig, I. Kammakakam, W. Falath and I. Kammakakam, *Mater. Adv.*, 2021, 2.
98 A. L. Hemasa, N. Naumovski, W. A. Maher and A. Ghanem, *Nanomaterials*, 2017, **7**, 1–32.
99 J. Yu, D. Huang, K. Huang and Y. Hong, *Chin. J. Chem.*, 2011, **29**, 893–897.
100 M. Ahmed, M. M. A. Yajadda, Z. J. Han, D. Su, G. Wang, K. K. Ostrikov and A. Ghanem, *J. Chromatogr. A*, 2014, **1360**, 100–109.
101 Y. Claude Guillaume and C. André, *Talanta*, 2013, **115**, 418–421.
102 X. Hua, Y. Du, J. Chen, G. Xu, T. Yu and Q. Zhang, *Electrophoresis*, 2013, **34**, 1901–1907.
103 Y. Moliner-Martínez, S. Cárdenas and M. Valcárcel, *Electrophoresis*, 2007, **28**, 2573–2579.
104 N. Na, Y. Hu, J. Ouyang, W. R. G. Baeyens, J. R. Delanghe, Y. E. C. Taes, M. Xie, H. Chen and Y. Yang, *Talanta*, 2006, **69**, 866–872.
105 Q. Zhang, Y. Du and S. Du, *J. Chromatogr. A*, 2014, **1339**, 185–191.
106 Y. Li, Q. Li, N. Zhu, Z. Gao and Y. Ma, *Chirality*, 2018, **30**, 996–1004.
107 T. Hong, X. Chen, Y. Xu, X. Cui, R. Bai, C. Jin, R. Li and Y. Ji, *J. Chromatogr. A*, 2016, **1456**, 249–256.
108 F. Y. Tu, L. Y. Yu, J. G. Yu, X. Q. Chen, Q. Fu, F. P. Jiao, Z. G. Peng and T. Zhang, *Nano*, 2013, **8**, 1350069.
109 R. Bhushan, S. Tanwar, R. Bhushan and S. Tanwar, *Biomed. Chromatogr.*, 2008, **22**, 1028–1034.
110 L. Candelaria, L. v. Frolova, B. M. Kowalski, K. Artyushkova, A. Serov and N. G. Kalugin, *Sci. Rep.*, 2018, **8**, 1–10.
111 Z. Liu, Y. Du and Z. Feng, *Microchim. Acta*, 2016, **184**, 583–593.
112 N. Ye, J. Li, Y. Xie and C. Liu, *Electrophoresis*, 2013, **34**, 841–845.
113 M. Cui, W. Zhang, L. Xie, L. Chen, L. Xu, I. Diaz and A. Garcia-Bennett, *Molecules*, 2020, **25**, 3899.
114 B. Di, L. Cheng, Q. Jiang, M. Su and W. Hao, *New J. Chem.*, 2013, **37**, 1603–1609.
115 P. Paik, A. Gedanken and Y. Mastai, *J. Mater. Chem.*, 2010, **20**, 4085–4093.
116 C. Casado, J. Castán, I. Gracia, M. Yus, Á. Mayoral, V. Sebastián, P. López-Ram-De-Viu, S. Uriel and J. Coronas, *Langmuir*, 2012, **28**, 6638–6644.
117 S. Lacasta, V. Sebastián, C. Casado, Á. Mayoral, P. Romero, Á. Larrea, E. Vispe, P. López-Ram-De-Viu, S. Uriel and J. Coronas, *Chem. Mater.*, 2011, **23**, 1280–1287.
118 P. Paik, A. Gedanken and Y. Mastai, *ACS Appl. Mater. Interfaces*, 2009, **1**, 1834–1842.

119 P. Paik, A. Gedanken and Y. Mastai, *Microporous Mesoporous Mater.*, 2010, **129**, 82–89.
120 M. X. Su, Z. Y. Liu, J. L. Chen, L. F. Cheng, B. Li, F. Yan and B. Di, *RSC Adv.*, 2014, **4**, 54998–55002.
121 W. Li, G. S. Ding and A. N. Tang, *RSC Adv.*, 2015, **5**, 93850–93857.
122 N. Na, Y. Hu, J. Ouyang, W. R. G. Baeyens, J. R. Delanghe and T. de Beer, *Anal. Chim. Acta*, 2004, **527**, 139–147.
123 C. Liu, B. Li and C. Xu, *Microchim. Acta*, 2014, **181**, 1407–1413.
124 Y. Sun, L. Zhang and H. Li, *New J. Chem.*, 2012, **36**, 1442–1444.
125 C. Liu, J. Lian, Q. Liu, C. Xu and B. Li, *Anal. Methods*, 2016, **8**, 5794–5800.
126 J. Wang and F. Liu, *Des. Monomers Polym.*, 2014, **17**, 19–25.
127 J. Huang, P. Su, B. Zhao and Y. Yang, *Anal. Methods*, 2015, **7**, 2754–2761.
128 C. L. Chang, X. Y. Qi, J. W. Zhang, Y. M. Qiu, X. J. Li, X. Wang, Y. Bai, J. L. Sun and H. W. Liu, *Chem. Commun.*, 2015, **51**, 3566–3569.
129 Y. Liu, A. Tian, X. Wang, J. Qi, F. Wang, Y. Ma, Y. Ito and Y. Wei, *J. Chromatogr. A*, 2015, **1400**, 40–46.
130 Y. Wei, A. Tian, Y. Li, X. Wang and B. Cao, *J. Mater. Chem.*, 2012, **22**, 8499–8504.
131 A. Tian, J. Qi, Y. Liu, F. Wang, Y. Ito and Y. Wei, *J. Chromatogr. A*, 2013, **1305**, 333–337.
132 A. P. Kumar, J. H. Kim, T. D. Thanh and Y. I. Lee, *J. Mater. Chem. B*, 2013, **1**, 4909–4915.
133 P. Qu, J. Lei, L. Zhang, R. Ouyang and H. Ju, *J. Chromatogr. A*, 2010, **1217**, 6115–6121.
134 H. J. Choi and M. H. Hyun, *Chem. Commun.*, 2009, 6454–6456.
135 G. D. Tarigh and F. Shemirani, *Talanta*, 2015, **144**, 899–907.
136 X. Weng, H. Bi, B. Liu and J. Kong, *Electrophoresis*, 2006, **27**, 3129–3135.
137 Q. Bai, C. Zhang, Y. Zhao, C. Wang, M. Maihemuti, C. Sun, Y. Qi, J. Peng, X. Guo, Z. Zhang and L. Fang, *Electrophoresis*, 2020, **41**, 1253–1260.
138 R. P. Liang, X. N. Wang, C. M. Liu, X. Y. Meng and J. D. Qiu, *J. Chromatogr. A*, 2014, **1323**, 135–142.
139 X. R. Yang, X. D. Song, H. Y. Zhu, C. J. Cheng, H. R. Yu and H. H. Zhang, *ACS Appl. Bio Mater.*, 2018, **1**, 1074–1083.
140 C. Aydoğan, V. Karakoç, F. Yılmaz, H. Shaikh and A. Denizli, *J. Biol. Chem.*, 2013, 29–36.
141 X. Dong, R. Wu, J. Dong, M. Wu, Y. Zhu and H. Zou, *Electrophoresis*, 2008, **29**, 3933–3940.
142 T. Wang, Y. Wang, Y. Zhang, Y. Cheng, J. Ye, Q. Chu and G. Cheng, *J. Chromatogr. A*, 2020, **1625**, 461284.
143 S. M. Xie, Z. J. Zhang, Z. Y. Wang and L. M. Yuan, *J. Am. Chem. Soc.*, 2011, **133**, 11892–11895.
144 Z. S. Gong, L. P. Duan and A. N. Tang, *Microchim. Acta*, 2015, **182**, 1297–1304.
145 J. Huang, P. Su, L. Zhou and Y. Yang, *Colloids Surf. A Physicochem. Eng. Asp.*, 2016, **490**, 241–249.
146 X. Sun, Y. Du, S. Zhao, Z. Huang and Z. Feng, *Microchim. Acta*, 2019, **186**, 1–7.
147 Y. Huang, X. Vidal and A. E. Garcia-Bennett, *Angew. Chem., Int. Ed. Engl.*, 2019, **58**, 10859–10862.